① 24/—258

第19卷第4期
2000年8月

红外与毫米波学报
J. Infrared Millim. Waves

Vol. 19, No. 4
August, 2000

DUAL-BAND INFRARED DETECTORS *

Rogal., A TN304.26 TN213

A. Rogalski **

(Institute of Applied Physics, Military University of Technology, 2 Kaliskiego St., 00-908 Warsaw, Poland)

Abstract As the infrared technology continues to advance, there is a growing demand for multispectral detectors for advanced IR systems with better target discrimination and identification. Both HgCdTe detectors and quantum well GaAs/AlGaAs photodetectors offer wavelength flexibility from medium wavelength to very long wavelength and multicolor capability in these regions. The main challenges facing all multicolor devices are more complicated device structtures, thicker and multilayer material growth, and more difficult device fabrication, especially when the array size gets larger and pixel size gets smaller. In the paper recent progress in development of two-color HgCdTe photodiodes and quantum well infrared photodetectors is presented.

More attention is devoted to HgCdTe detectors. The two-color detector arrays are based upon an n-P-N (the capital letters mean the materials with larger bandgap energy) HgCdTe triple layer heterojunction design. Vertically stacking the two p-n junctions permits incorporation of both detectros into a single pixel. Both sequential mode and simultaneous mode detectors are fabricated. The mode of detection is determined by the fabrication process of the multilayer materials.

Also the performances of stacked multicolor QWIPs detectors are presented. For multicolor arrays, QWIP's narrow band spectrum is an advantage, resulting in low spectral crosstalk. The major challenge for QWIP is developing broadband or multicolor optical coupling structures that permit efficient absorption of all required spectral bands.

Key words n-P-N HgCdTe photodetectors, QWIPs, dual-band detectors, sequential and simultaneous operations, focal plane arrays

Introduction

Multicolor capabilities are highly desirable for advance infrared (IR) systems. Systems that gather data in separate IR spectral bands can discriminate both absolute temperature and unique signatures of objects in the scene. By providing this new dimension of contrast, multiband detection also enables advanced color processing algorithms to further improve sensitivity above that of single-color devices. This is extremely important for the process of identifying temperature difference between missile target, war heads and decoys. Multispectral IR focal plane arrays (FPAs) can also play many important roles in earth and planetary remote sensing, astronomy, etc.

Currently, multispectral systems rely on cumbersome imaging techniques that either disperse the optical signal across multiple IR FPAs or use a filter wheel to spectrally discriminate the image focused on single FPA. These systems contain beam-splitters, lenses and bandpass filters into the optical path to focus the images onto separate FPAs responding to different IR bands. Also complex alignment is required to map the multispectral image pixel for pixel. Consequently, these approaches are expensive in terms of size, complexity, and cooling requirements.

At present considerable efforts are directed to fabricate a single FPA with multicolor capability to eliminate the spatial alignment and temporal registration problems that exist whenever separate arrays are used. This "integration" of multispectral capability affords sensitivity to different IR bands within each

* This work was partially supported by the Polish State Committee for Scientific Research under grant number PBZ 28.11/P6
Received 2000-01-14

** e-mail: rogan@wat.wew.pl

* 受到波兰国家科学研究委员会部分资助(PBZ28.11/P6)
稿件收到日期 2000-01-14

and every unit cell of the array so that temporal and spatial co-registration between each spectral field now occurs on the pixel level. This approach offers multicolor advantages without the complexity of multiple FPA systems, thereby offering significant reduction of weight and power consumption in a simpler, more reliable and less costly package. They can be implemented as a capability upgrade to existing single color systems with only minor modifications to FPA control and signal processing electronics, since power and space requirements for multispectral FPAs are identical to single-color FPAs. It is expected that beyond five years, as the two-color array technology in demonstration currently moves into production, there will be demonstrations of three- and four-color capabilities squeezed into pixel. Four colors may be about the limiting number of bands that can be stacked in a single pixel. For applications desiring greater spectral decomposition, alternative approaches are being developed[1,2].

Both HgCdTe photodiodes and quantum well infrared photodetectors (QWIPs) offer the multicolor capability in the middle wavelength IR (MWIR) and long wavelength IR (LWIR) range. Each of these technologies has its advantages and disadvantages. QWIP technology is based on the well developed A^3B^5 material system which has a large industrial base with a number of military and commercial applications. Therefore QWIPs are easier to fabricate with high yield, high operability, good uniformity and lower cost. HgCdTe material system is only used for detector applications. On the other hand, HgCdTe FPAs have higher quantum efficiency, higher operating temperature and potential for the highest performance. A more detailed comparison of both technologies has been recently given by Tidrow *et al.* and Rogalski[3,4]. They compared the technical merits of two IR detector arrays technologies: photovoltaic HgCdTe and QWIPs. It was clearly shown that long wavelength IR (LWIR) QWIP cannot compete with HgCdTe photodiode as the single device especially at higher temperature operation (>70K) due to fundamental limitations associated with intersubband transitions. However, the advantage of HgCdTe is less distinct in temperature range below 50K due to problems involved in HgCdTe material (p-type doping, Shockley-Read recombination, trap-assisted tunneling, surface and interface instabilities). Even though QWIP is a photoconductor, its several properties such as high impedance, fast response time, long integration time, and low power consumption, well comply with requirements of fabrication of large FPAs. Due to the high material quality at low temperature, QWIP has potential advatages over HgCdTe for very LWIR (VLWIR) FPA applications in terms of the array size, uniformity, yield and cost of the systems.

Considerable progress has been recently demonstrated by research groups at Hughes Research Laboratory[5~8] and Lockheed Martin[9~12] in multispectral HgCdTe detectors employing MBE and MOCVD for the growth of varieties of devices. Also QWIP's technology demonstrates considerably progress in fabrication of multicolor FPAs[12~15]. Devices for the sequential and simultaneous detection of two closely spaced sub-bands in MWIR and LWIR radiation have been demonstrated.

The paper summarized here is a culmination of recent progress in critical technologies necessary for multicolor detector development. This paper reviews recent progress made in two-color detector technology from the infrared industrial community.

1 HgCdTe dual-band detectors

The unit cell of an integrated two-color FPAs consists of two co-located detectors, each sensitive to a different spectral band. Radiation for both bands is incident on the shorter band detector, with the longer wave radiation passing through to the second detector. This device architecture is realized by placing a longer wavelengh HgCdTe photodiode simply behind shorter wavelength photodiode. Back-to-back photodiode two-color detectors were first implemented using quaternary Ⅲ-Ⅴ alloy ($Ga_xIn_{1-x}As_yP_{1-y}$) absorbing layers in a lattice matched InP structure sensitive to two different short wavelength IR (SWIR) bands[16]. Integrated two-color technology HgCdTe has been developed at Santa Barbara Re-

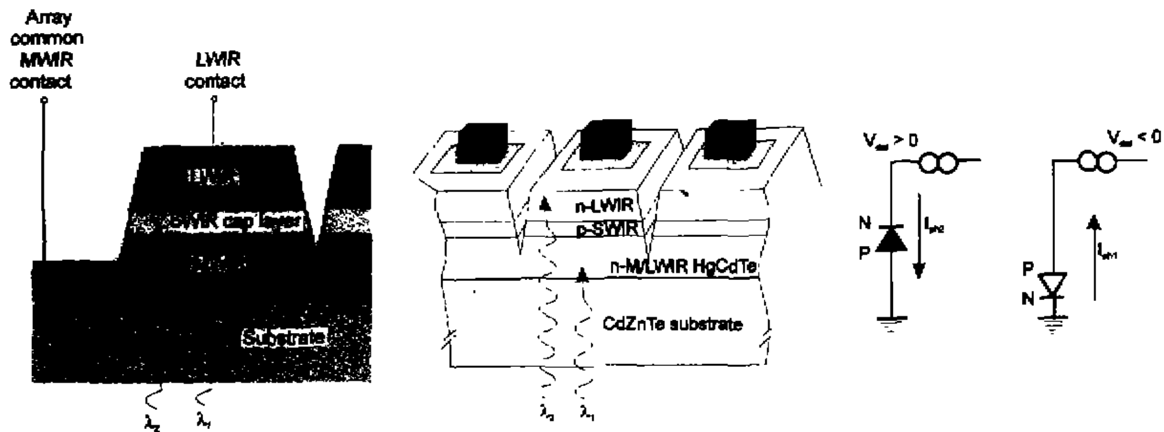

Fig. 1 Schematic cross section of integrated photovoltaic two-color detectors in an n-P-N layer structure for sequential operating mode

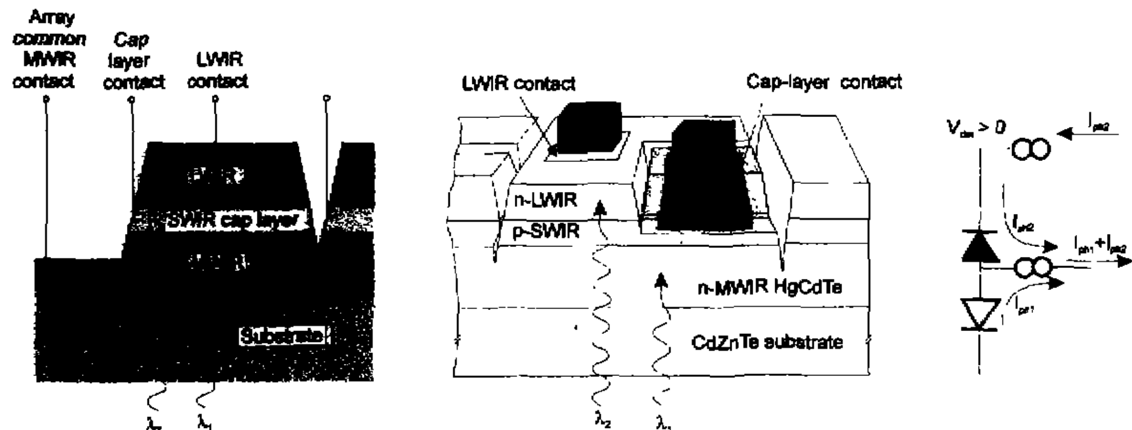

Fig. 2 Schematic cross section of integrated photovoltaic two-color detectors in an n-P-N layer structure for simultaneous operating mode

search Center (SBRC), Rockwell and Lockheed Martin for nearly a decade with a steady progression having a wide variety of pixel size (30 to 61μm), array formats (64×64 up to 320×240) and spectral-band sensitivity (MWIR/MWIR, MWIR/LWIR) and LWIR/LWIR[8]. Following the successful demonstration of multispectral detectors in liquid phase epitaxy(LPE)-grown HgCdTe devices[17], the MBE and MOCVD techniques have been used for the growth of a variety of multispectral detectors.

1.1 Sequential and simultaneous operation

The two-color detector arays are based upon an n-P-N (the capital letters mean the materials with larger bandgap energy) HgCdTe triple layer hetero-junction (TLHJ) design. The TLHJ detectors consist of back-to-back photovoltaic p-n junctions. Vertically stacking the two p-n junctions permits incorporation of both detectors into a single pixel.

Both sequential mode and simultaneous mode detectors are fabricated from the multi-layer materials. The mode of detection is determined by the fabrication process. Figures 1 and 2 show the elements of arrays of two-color photovoltaic unit cells in both modes. The simultaneous mode requires bias contact to the cap layer (Fig. 2), while the sequential mode does not (Fig. 1). The sequential-mode detector has a single indium bump per unit cell that permits sequential bias-selectivity of the spectral bands associated with operating tandem photodiodes. The simultaneous mode detector employs an additional electrical contact to the shared-type centre layer so that each junction can be accessed independently with

both signal channels integrated simultaneously. The two indium bumps per unit cell required for the simultaneous mode detectors can be fabricated in relatively small unit cells with high optical fill factor.

Thus, two-color HgCdTe FPAs present considerable challenges in three technology arrays. First, a versatile multilayer growth capability is needed to form heterojunctions. Second, fairly sophisticated array processing technology is needed to make tight-geometry features, such as two bumps per unit cell and insulated over-the-edge contact metallizations, in unit cells as small as $40 \times 40\mu m^2$. Third, the silicon readout integrated circuit (ROIC) chip now requires two input circuits per unit cell.

The distinguishing feature of sequential approach is that the p-type cap layer is not contacted. Elimination of the contact has several key advantages[17].

- Only one in-cell indium contact is required, giving a unit cell the simplicity of a single-color array.
- Only one readout per unit cell is required, providing space for higher performance readouts.
- The simple structure provides smaller and more producible unit cells ($<40\mu m$).
- Near 100% fill factor can be achieved in both colors (there are no compound features to disrupt total internal reflection of the LWIR signal and no second-plane circuitry to obscure incident radiation).
- Each detector is precisely co-located since no part of the LWIR detector must be given up to form a cap layer contact.

Critical step in device formation is connected with *in situ* doped p-type As-doped layer with good structural and electrical properties to prevent internal gain from generating spectral crosstalk. The bandgap engineering effort consists of increasing the CdTe mole fraction and the effective thickness of the p-type layer to suppress out-off-band carriers from being collected at the terminal.

The problems with the bias selectable device are the following: its construction does not allow independent selection of the optimum bias voltage for each photodiode, and there can be substantial medium wavelength (MW) crosstalk in the long wavelength (LW) detector. To overcome the problems of the bias-selectable device, the independently accessed back-to-back photodiode dual-band detectors have been proposed. An implementation of the simultaneous mode using a second indium bump in the unit cell is shown in Fig. 3. The mesa shape has become more complicated to provide access to the cap layer for the third contact. Internal gain is very effectively suppressed through proper bias of each diode, easing the design and growth emphasis on bandgap engineering. The most important distinction is the requirement of a second readout circuit in each unit cell. Longwave band fill factor is reduced from that of the midwave, since some junction area is sacrificed to provide contact to the buried cap layer, and spatial coincidence is altered. The difference between sequential and simultaneous operation becomes to some extent indistinct when two widely separated spectral bands are used, such as the $3\sim5\mu m$ and $10\sim12\mu m$ bands. Photon fluxes in the longer wavelength band are generally much higher than in the shorter wavelength band, requiring a significantly shorter integration time for the longwave band, and loss of true simultaneity of signal integration can occur. In this situation a smaller LWIR fill factor can be a benefit in reducing background-generated charge.

It should be noticed that two-color detector arrays are also connected to the ROIC by vias (see Fig. 4) and not by commonly used indium bumps. This

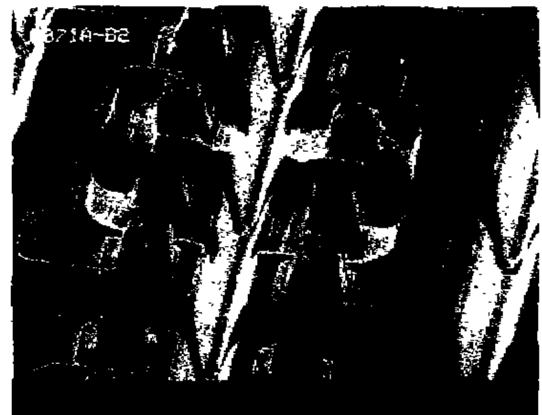

Fig. 3 SEM photo of a 64×64 two-color HgCdTe detector array with $75\times75\mu m^2$ unit cells (after Ref. 11)

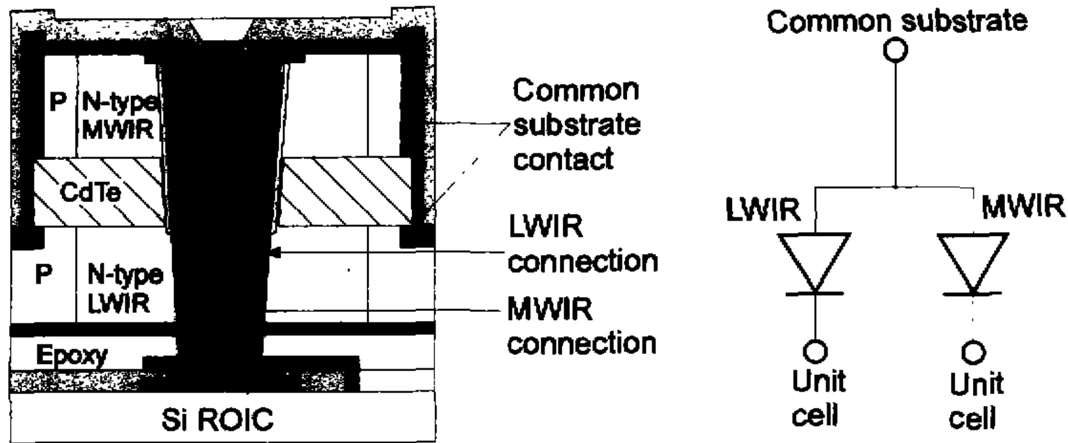

Fig. 4 Two-color HgCdTe detector connected to the ROIC by vias (after Ref. 12)

technique has been successfully used by Raytheon TI systems for their single color IR FPAs.

Reine and co-workers[10,11] have proposed a novel simultaneous MWIR/LWIR dual-band HgCdTe detector fabricated from a P-n-N-P layers grown *in situ* by the interdiffused multilayer process (IMP) MOCVD onto lattice-matched CdZnTe substrates. Figure 5 shows cross section of the independently accessed back-to-back photodiode dual-band detector. The LW photodiode is a P-on-n heterojunction, grown directly on top of the MW photodiode, which is an n-on-P heterojunction. A thin n-type compositional barrier layer is placed between the MW and LW absorber layers. This barrier layer forms isotype n-N heterojunction at the interface, which prevents MW photocarriers from diffusing into the LW absorber layer and prevents LW photocarriers from diffusing into the MW absorber layer.

In dual-band IR hybrid FPAs with the above detectors, one bump contacts only the p-type region of the LW photodiode; the other bump contacts the n-type region of the LW photodiode, and therefore also the n-type region of the MW photodiode, through an over-the-edge metalization. In this way the LW photodiode is accessed directly through the two bumps, while the MW photodiode is accessed through the contact to the n-type egion and the array ground. This dual-band device showed that the MW N-on-P homojunction photodiodes had good R_oA products [$R_0=dI/dV)^{-1}$ at bias voltage $V=0$, and A is the detector area] but the quantum efficiencies were anomalously low and in come cases the spectral responses were sharply peaked. To alleviate these problems, *in situ* growth of MW diodes in the N-on-P heterojunction configuration by MOCVD has been carried out[10,11] (see structure shown in Fig. 5). In the N-on-P heterojunction, the absorber layer is the n-type layer as compared to the p-type layer in the N-on-P homojunction, and significantly improved quantum efficiency of 65~80% (without anti-reflection coating) and classical spectral response have been obtained.

1.2 Technology and characterization of multilayer heterojunctions

Sharp turn off of the detector's special response, a feature which is necessary to achieve low crosstalk in either bands, requires the growth of homogeneous n-type absorber layer at the predetermined alloy composition. Other detector requirements are high quantum efficiency (above 70%) in both bands and high R_oA product. To satisfy these requirements it is necessary to have precise control over the placement of the electrical junction, which is determined by location of the arsenic dopant profile with respect to that of In in a heterojunction. Due to the nature of the growth process, the capabilities to control and tailor the alloy composition and the dopant profiles are in principle possible by MBE and MOCVD.

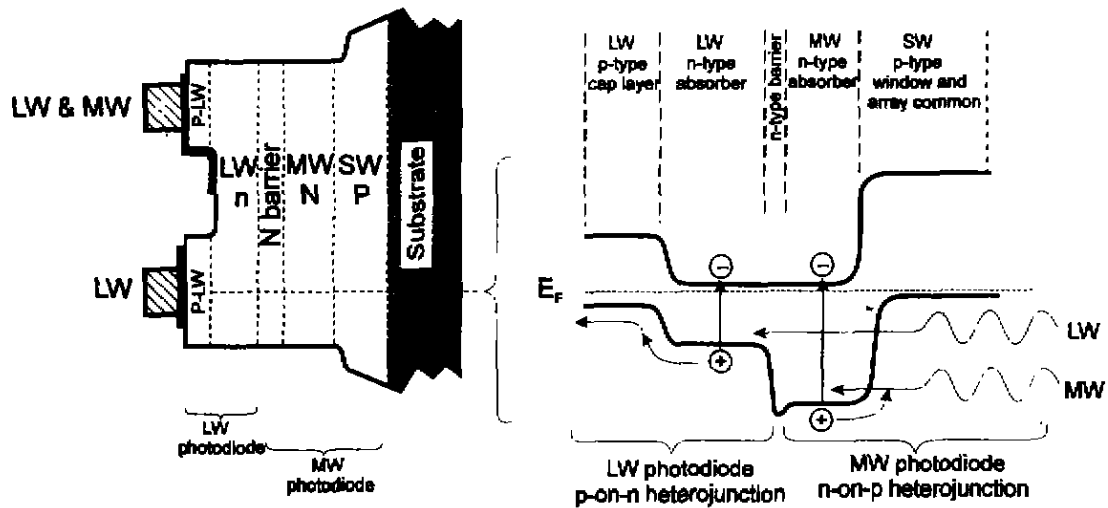

Fig. 5 Cross section and energy band profile of the independently accessed back-to-back HgCdTe photodiode dual-band detector (after Ref. 11)

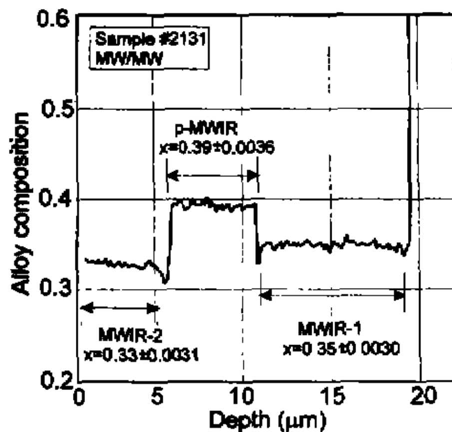

Fig. 6 SIMS profile showing the composition in layers with three distinct MWIR compositions (after Ref. 6)

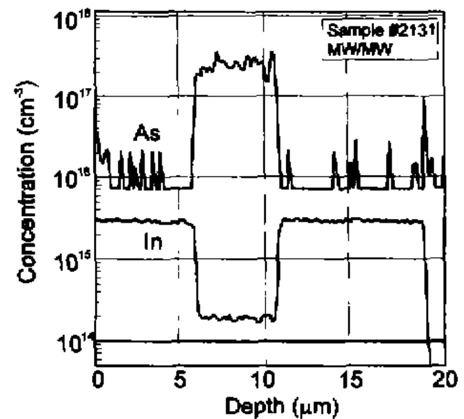

Fig. 7 SIMS profiles for In and As in n-P-N structure (after Ref. 7)

Two-band HgCdTe detectors are usually fabricated from n-P-N layers grown *in situ* by MBE or MOCVD onto lattice-matched CdZnTe substrate. Using MBE growth, the precision in the x-value is about ± 0.005[7]. For MWIR layers, a variation in the x-value of 0.005 produces a change in the cutoff of 0.01μm at 77K. The cutoff wavelength of each junction is controlled by varying the composition of the HgCdTe used in the layers. The thickness of the absorber layers is optimized for near unity quantum efficiency and low dark current. This is achieved with a layer thickness slightly higher than the inverse absorption coefficient $1/\alpha$ (which is near 10μm). Figure 6 shows the three distinct compositions corresponding to the MBE grown n-P-N layers observed in the representative SIMS profile. The average alloy composition in the 6μm thick MWIR-1 layer is $x = 0.35$ with standard deviation of 0.0030 (i.e. standard deviation of $<1\%$) and the corresponding values of the 6μm thick MWIR-2 is 0.33 ± 0.0031. The dip in the x-value at the two p/n interfaces seen in Fig. 6 is a result of the change in the alloy composi-

tion as a result of a reduction in the growth temperature for the growth of the p-type layer. This reduction in growth temperature is required to facilitate incorporation of adequate amounts of As acceptor impurities in the p-type layer.

Low doping is beneficial for a low thermal generation and high quantum efficiency. The n-type base absorbing regions are deliberately doped with indium at a level of about $(1\sim3)\times10^{-15}cm^{-3}$. The p-n junctions are formed using arsenic as the dopant at a level of about $10^{18}cm^{-3}$. To activate As as an acceptor, it must occupy a Te site in the lattice. Full As activation is achieved for annealing temperature of 300℃ or higher, followed by an annealing at 250℃ in Hg pressure to annihilate Hg vacancies. Figure 7 shows SIMS profiles for In and As in an n-P-N structure. As-grown layers exhibit constant levels of In in the two n-type absorber layers, and the As profile exhibits sharp turn on and turn off in the intermediate p-type layer. Furthermore, the In and As profiles indicate negligible dopant diffusion during growth.

One key technical issue in epi-growth of two-color HgCdTe detectors is high dislocation densities. The commercially available $Cd_{0.96}Zn_{0.04}Te$ substrates are lattice-matched to LWIR-$Hg_{1-x}Cd_xTe$ with $x=0.22$. $Hg_{0.78}Cd_{0.22}Te$ grown on $Cd_{0.96}Zn_{0.04}Te$ substrates exhibit an average etch-pit density (EPD) of about $5\times10^5cm^{-2}$ in as-grown layers. Rajavel *et al*[7]. have observed that MWIR-HgCdTe ($x=0.30\sim0.35$) layers which deposited on $Cd_{0.96}Zn_{0.04}Te$ substrates, on average, exhibit an EPD that is a factor of 5~10 higher than the LWIR-HgCdTe. The increased EPD in the MWIR-HgCdTe is a result of the lattice mismatch with the substrate, which is as small as 0.04%. Figure 8 shows the near-surface EPD measured in as-grown MWIR/MWIR two-color detector structure. The layers in each of the two sets were grown consecutively. It should be noticed, however, that the R_oA product of MWIR detectors at 77K is not affected by the dislocation density at levels about $5\times10^6cm^{-2}$. The performance of LWIR-HgCdTe photodiodes at low temperature (40K below) is expected to be strongly dependent on the EPD in the absorber layer[15]. For LWIR photodiodes at 78K, the R_oA product begins to decrease at dislocation density of approximately 10^5cm^{-2}[15,19].

Four-layer P-n-N-P structures have been grown on nominally lattice matched CdZnTe (100) 4~8° misoriented toward (111) B. Improvements in MOCVD-IMP were incorporated along with the use of iodine donors and more classical p-type doping with arsenic from DMAAs. The 8-μm thick p-layer was grown first (see Fig. 5), with an x-value of 0.40 and doped with arsenic at $(1\sim3)\times10^{17}cm^{-3}$. The near 8μm thick MW n-type absorber layer was grown next and doped with iodine at $(2\sim4)\times10^{15}cm^{-3}$.

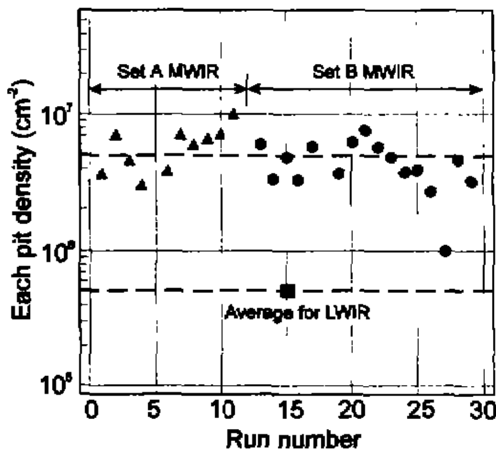

Fig. 8 The near-surface etch-pit density in MWIR/MWIR two-color detector structures (after Ref. 7)

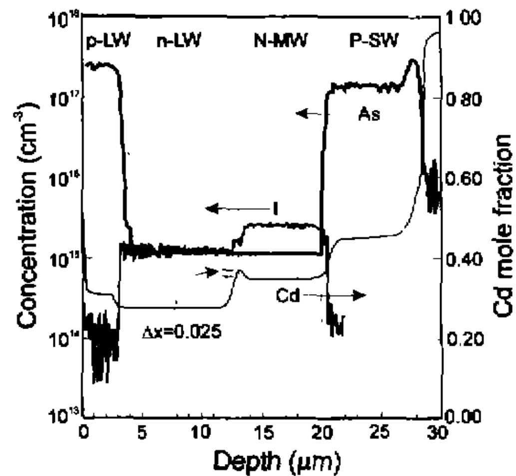

Fig. 9 SIMS data for a four-layer P-n-N-P structure grown *in situ* by IMP-MOCVD (after Ref. 11)

Next a small compositional barrier has been added at the MW/LW absorber layer interface. This was followed by the n-type LW absorber layer, 8～10μm thick and doped with iodine at $(1-2)\times10^{15}cm^{-3}$, on which a 2μm tick p-type layer, doped with arsenic at $(1-3)\times10^{17}cm^{-3}$, was grown. The bandgap of the p-type cap layer was wider than that of the n-type absorber layer, with $\Delta x=0.04$. The growth run was terminated with a thin CdTe layer (0.15μm) to prevent outdiffusion of Hg during the interdiffusion annealing and cooldown. Finally, the HgCdTe layers were annealed under Hg-rich conditions for arsenic activation. In the FPA, the wide gap SW p-type layer is the common contact to all detectors in the array. Figure 3 shows a scanning electron micophotograph of a section of a 64×64 dual-band HgCdTe detector array. The 23μm deep MW mesas were defined by ECR dry etching. Figure 9 shows SIMS data for the iodine donors, the arsenic accepors, and the HgCdTe alloy composition. Note the abruptness of the transitions between the various layers, which illustrates the excellent control of donor and acceptor concentrations and of alloy composition.

1.3 State of the art of two-color HgCdTe detectors

Integrated two-color detectors have been implemented in a number of variations of structure and material for operation in either sequential or simultaneous mode. Figure 10 shows examples of spectral response from MWIR/MWIR, MWIR/LWIR, and LWIR/LWIR two-color devices. Note that there is a minimal crosstalk between the bands since the short wavelength band absorbs nearly 100% of the shorter wavelengths. One might ask whether the additional processing and complexity of building a two-color detector structure may adversely affect the performance, yield, or operability of two-color devices. Test structure indicates that the separate photodiodes in a two-color detector perform exactly as single-color detectors in terms of achievable R_oA product variation with wavelength at a given temperature.

The simultaneous mode two-color detectors were delineated as mesa isolated structures and contacts were made to the top n-type layer and the intermediate p-type layer. Fill factors of 128×128 MWIR/MWIR FPAs as high as 80% were achieved by using a single mesa structure to accommodate the two indium bump contacts required for each unit cell with 50μm size. The bottom n-type layer served as the common ground. Figure 11 shows the uniformity of responsivity for each of the bands. Band 1(2.5～3.9μm) had operability of 99.9%, with 23 inoperable pixels. Band 2(3.9～4.6μm) had operability of 98.9%, with 193 inoperable pixels. Quantum efficiencies of 70% were observed in each band without using an anti-reflection coating. The R_oA values for the diodes ranged from 8.25×10^5 to $1.1\times10^6\Omega cm^2$ at f/2 FOV. The NEDT for both bands as a function of temperature is shown in Fig. 12. The camera used for these measurements had a 50mm, f/2.3 lens. Imagery was acquired at temperatures as high as 180K with no visible degradation in image quality.

The experimentally demonstrated 64×64 MW/LW dual-band MOCVD HgCdTe array is characterized in Table 1. The array has a unit cell size of 75×

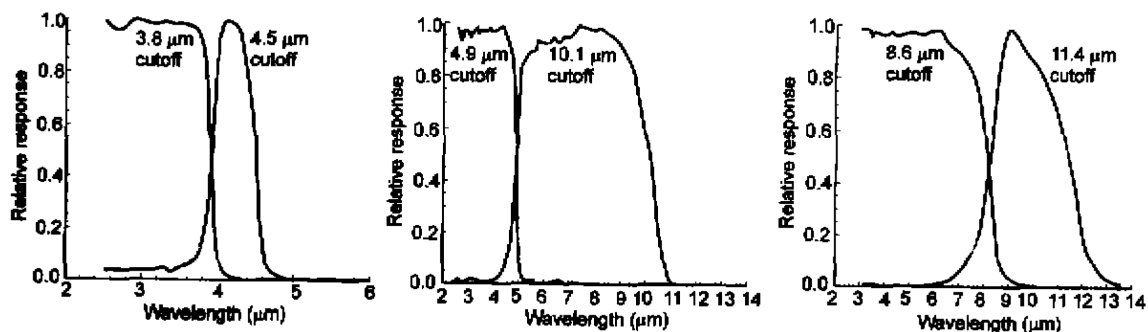

Fig. 10 Spectral response curves for two-color HgCdTe detectors in various dual-band combinations of MWIR and LWIR spectral bands (after Ref. 1)

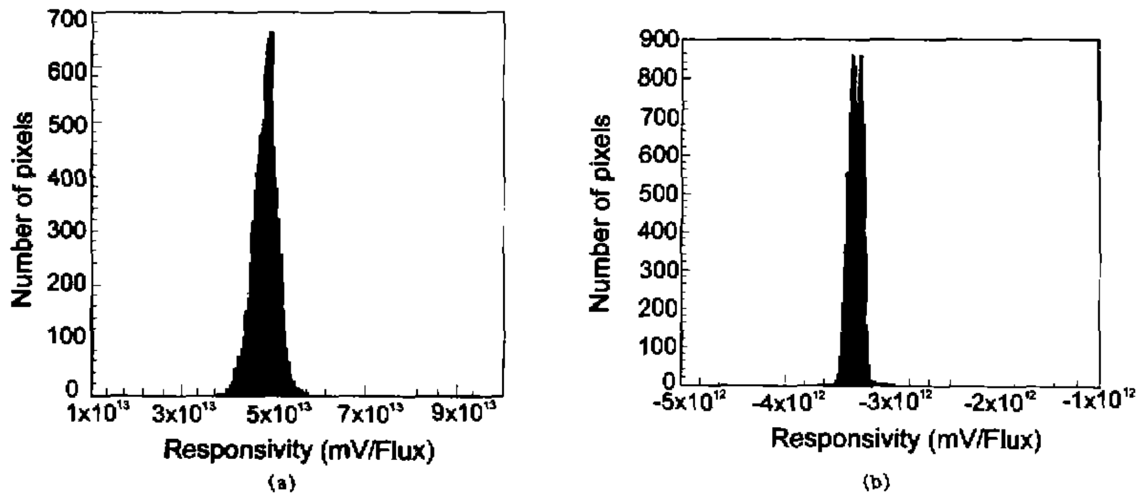

Fig. 11 Responsivity uniformity for 2.5~3.9μm band (a) and 3.9~4.6μm band (b) (after Ref. 1)

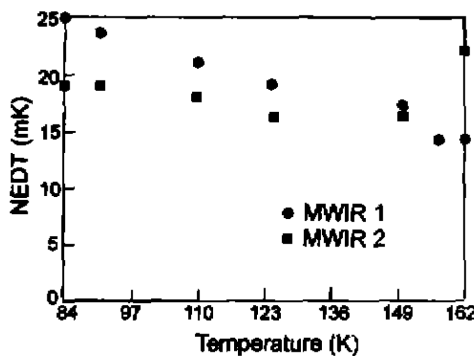

Fig. 12 Noise-equivalent difference temperature for two-color camera having 50mm, f/2.3 lens, as a function of operating temperature (after Ref. 1)

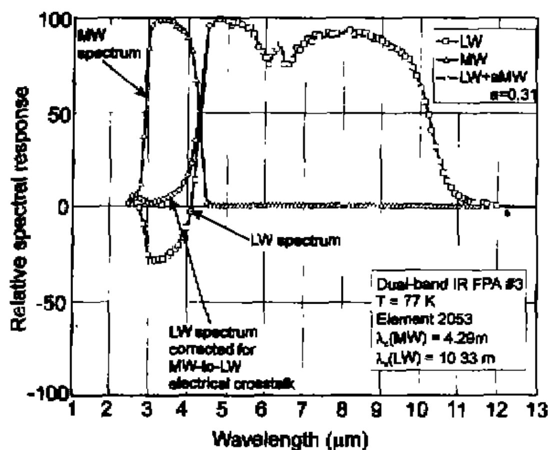

Fig. 13 Relative spectral response data at 78K for the MW and LW detectors in one of the dual-band detectors in 64×64 dual-band FPA (after Ref. 11)

75μm^2. The arrays were hybridized to a dual-band silicon multiplexer readout chip that allowed the MW and LW photocurrents to be integrated simultaneously and independently. The MW and LW average cutoff wavelengths at 77K are in the 4.27~4.35μm and 10.1~10.5μm ranges, respectively. Figure 13 shows the relative spectral response data at 78K for the MW and LW detectors in one of the dual-band FPA. The MW response is quite small for wavelengths beyong 4.5μm, indicating low LW-to-MW crosstalk (defined as the ratio of the MW photocurrent to the LW photocurrent when only LW radiation is incident on the detector), consistent with the measured crosstalk value of 0.4%. The MW response at wavelength less than 2.9μm is suppressed, presumably due to a high recombination rate for SW photocarriers at the interface between the wide-gap p-type window layer and the CdZnTe substrate (see Fig. 5). The expected filtering of the LW photodiode response spectrum by the MW layer is clearly evident in the sharp increase in LW response at 4.3μm. The measured LW response spectrum is negative at those wavelengths for which the MW response is high, which is attributed to electrical crosstalk due to finite series resistance in the input circuit[11]. A simple small-signal model for this crosstalk mechanism predicts that the crosstalk is given by $R_s/(R_L+2R_s)$, where R_L is the dynamic resistance of the LW diode and R_s is the impedance of the input circuit. There are two approaches for reducing this MW-to-LW electrical crosstalk: increas-

Table 1 Summary of performance data for 64×64 MW/LW dual-band HgCdTe FPA (after Ref. 11)

Parameter	MW	LW
Cutoff wavelength (avg[σ/μ])(μm)	4.27[0.5%]	10.1[2.2%]
Quantum efficiency (avg[σ/μ])	79%[9%]	67%[29%]
Detectivity (f/2.9)(median) (cmHz$^{1/2}$/W)	4.8×10^{11}	7.1×10^{10}
NEDT (T_{SCENE}=295K, τ_{INT}=2.2ms)(median)(mK)		
measured: f/2.9, MW: 3.0~4.35μm, LW: 4.5~10.1μm	20	7.5
projected: f/2.9, MW: 3.0~4.35μm, LW: 7.0~10.1μm	12	6.2
Stare efficiency	87%	87%
Fill factor = A_{OPT}/(75×75μm^2)	94%	39%
Dynamic range (average)(dB)	77	75
Dynamic resistance R_D(average)(Ω)	4.2×10^{9}	2.3×10^{6}
R_DA_{OPT}(average)(Ωcm^2)	2.4×10^{4}	51
Spectral crosstalk		
LW (7−11μm)→MW	0.4%	
MW(4.0μm)→LW		−10%

All data were measured at the temperature of 78K. Signal response was measured with an MW notch filter at 4.0μm or an LW filterat 7~11μm. Average values for all 64×64 elements are stated for all parameters except detectivity and NEDT, for which the median values are quoted.

ing the LW photodiode dynamic resistance R_L by improving junction quality, and reducing series resistance R_s by replacing the direct injection circuit with, for example, a buffered direct injection circuit.

These staring dual-band FPAs exhibit high average quantum efficiency (MW: 79%; LW: 67%), high median detectivities (MW: 4.8×10^{11} cmHz$^{1/2}$W^{-1}; LW: 7.1×10^{10} cmHz$^{1/2}$W^{-1}), and low median NEDTs (MW: 20mK; LW: 7.5mK for T_{SCENE} = 295K and f/2.9).

2 Dual-band QWIPs

Despite large research and development efforts, large photovoltaic HgCdTe FPAs remain expensive, primarily because of the low yield of operable arrays. The low yield is due to sensitivity of LWIR HgCdTe devices to defects and surface leakage, which is a consequence of basic material properties. With respect to HgCdTe detectors, GaAs/AlGaAs quantum well devices have a number of potential advantages, including the use of standard manufacturing techniques based on mature GaAs growth and processing technologies, highly uniform and well-controlled MBE growth on GaAs wafers greater than 6 in., high yield and thus low cost, more thermal stability, and intrinsic radiation hardness. In the commercial arena and in some military applications where ultimate performance is not required, QWIPs have a big advantage in terms of cost. These detectors are extrinsic devices in which the dopant concentrations are limited by the epitaxial growth processes. In addition, the intersubband lifetimes in multiquantum well (MQW) detectors are inherently short (about 10^{-11} s), which results in low quantum efficiency and relatively poor performance at temperatures higher than 40K. At the higher temperatures, thermally excited carriers dominate optically produced carriers, resulting in a low signal-to-noise ratio. However, the signal-to-noise ratio is usually sufficient for the most common imaging applications. Due to the inherent properties such as narrow-band response, wavelength tailorability, and stability (i.e. low $1/f$ noise) associated with GaAs based QWIPs, it is an ideal candidate for large format multicolor FPAs.

2.1 Operation of QWIPs

All QWIPs are based on "bandgap engineering" of layered structure of wide bandgap (relative to thermal IR energies) materials. The structure is designed such that the energy separation between two of the states in the structure matches the energy of the infrared photons to be detected. Several QWIP configurations have been reported based on transitions from bound-to-extended states, bound-to-quasicontiuum states, bound-to-quasibound states, and bound-to-miniband states.

Figure 14 shows two detector configurations

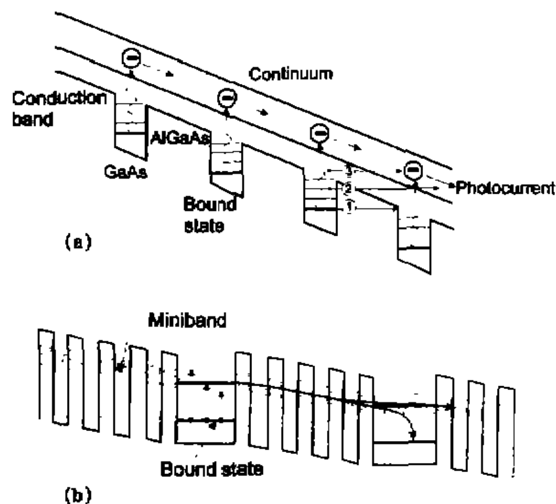

Fig. 14 Schematic band diagram of demonstrated QWIP structures: (a) bound-to-extended and (b) bound-to-miniband. Three mechanisms creating dark current are also shown in Fig. 14 (a): ground-state sequential tunneling (1), intermediate thermally assisted tunneling (2), and thermionic emission (3). The gray indicates extended states through which current flows

used in fabrication of two-color QWIP FPAs. The major advantage of the bound-to-continuum QWIP is that the photoelectron can escape from the quantum well to the continuum transport states without being required to tunnel through the barrier. As a result the voltage bias required to efficiently collect the photoelectrons can be reduced dramatically, thereby lowering the dark current. Furthermore, since the photoelectrons do not have to tunnel through them, the AlGaAs barriers can be made thicker without reducing the photoelectron collection efficiency. It appears that the dark current decreases significantly when the first excited state is dropped from the continuum to the well top, bound-to-quasibound QWIP, without sacrificing the responsivity.

A miniband transport QWIP contains two bound states with higher energy level being resonance with the ground state miniband in the superlattice barrier [see Fig. 14(b)]. In this approach, IR radiation is absorbed in the doped quantum wells, exciting an electron into the miniband and transporting it in the miniband until it is collected or recaptured into another quantum well. Thus the operation of this miniband QWIP is analogous to that of a wealy coupled MQW bound-to-continuum QWIP. In this device structure, the continuum states above the barriers are replaced by the miniband of the superlattice barriers. The miniband QWIPs show lower photoconductive gain than bound-to-continuum QWIPs because the photoexcited electron transport occurs in the miniband where electrons have to transport through many thin heterobarriers resulting in a lower mobility. Beck and Faska[13-14] adopted this bound-to-miniband approach and demonstrated excellent IR images from 256 × 256 FPA camera. Sanders was first to fabricate two-color, 256 × 256 bound-to-miniband QWIP FPAs in each of four important combinations: LWIR/LWIR, MWIR/LWIR, near IR (NIR)/LWIR and MWIR/MWIR-with simultaneous integration[14].

A key factor in QWIP FPA performance is the light-coupling scheme. Different light-coupling mechanisms are used in QWIPs. A distinct feature of QWIPs is that the optical absorption strength is proportional to an incident photon's electric-field polarization component normal to the quantum wells. This implies that a photon propagating normal to the quantum wells, whose polarization is entirely in the plane of the quantum wells, is not absorbed. Therefore, these detectors have to be illuminated through a 45° polished facet. For imaging, it is necessary to be able to couple light uniformly to two-dimensional (2-D) arrays of these detectors, so a diffraction periodic grating[20] or other similar structure (such as random reflectors[21], corrugated reflectors[22], lattice mismatch strain material systems, and p-type materials[23]) is typically fabricated on one side of the detectors to redirect a normally incident photon into propagation angles more favorable for absorption. Most QWIP arrays use 2-D grating, which is very wavelength-dependent, and efficiency gets lower when the pixel size gets smaller. Lockheed Martin has used rectangular and rotated rectangular 2-D gratings for their two-color LW/LW FPAs. Although random reflectors have achieved relatively high quantum effi-

ciencies with large test device structure, it is not possible to achieve the similarly high quantum efficiencies with random reflectors on small FPA pixels due to the reduced width-to-height aspect rations. In addition, it is difficult to fabricate random reflectors for shorter wavelength detectors relative to long wavelength detectors due to the fact that feature sizes of random reflectors are linearly proportional to the peak wavelength of the detectors. As a result, the quantum efficiency becomes a more difficult issue for QWIP multicolor FPA than for single color.

2.2 State of the art of dual-band QWIPs

Device capable of simultaneously detecting two separate wavelengths can be fabricated by vertical stacking of the different QWIP layers during epitaxial growth. Separate bias voltages can be applied to each QWIP simultaneously via the doped contact layers that separate the MQW detector heterostructures. Figure 15 shows schematically the structure of a two-color stacked QWIP with contacts to all three ohmic-contact layers. The device epilayers were grown by MBE on 3-inch semi-insulating GaAs substrate. An undoped GaAs layer, called an isolator, was grown between two AlGaAs stop layers, followed by an ohmic contact of 0.5μm thick doped GaAs layer. Next, the two QWIP heterostructures were grown, separated by another ohmic contact. All contact layers were doped to $n=1\times10^{18}cm^{-3}$. The long wavelength sensitive stack (red QWIP, $\lambda_c=11.2\mu m$) is grown above the shorter wavelength sensitive stack (blue QWIP, $\lambda_c=8.6\mu m$.). Each QWIP is a 20-period GaAs/Al_xGa_{1-x}As MQW stack, in which the thickness of the Si-doped GaAs QWs (with typical electron concentration $5\times10^{17}cm^{-3}$) and the Al composition of the undoped Al_xGa_{1-x}As barriers (≈550−600 Å) are adjusted to yield the desired peak position and spectral width.

The top surface shown in Fig. 15 is patterned with a regular 2-D optical coupler, using reactive etching. A 256×256 pixel array (pitch = $40\times40\mu m^2$, pixel size = $39\times39\mu m^2$) was defined, and the etching was performed down to the upper stop layer to ensure electrical and optical isolation of each pixel from its neighbors. Each pixel was also etched to allow metal contacts to be attached to the different ohmic contact layers. Usually Au/Ge contacts were evaporated onto the top, middle, and bottom contact layers. After this step indium bumps, three per pixel, were placed on the metal contact pads (Fig. 16). The wafer was diced, and suitable arrays were hybridized to a CMOS readout IC. The gaps between FPA detectors and the readout multiplexer were backfilled with epoxy. The epoxy backfilling provides the necessary mechanical strength to the detector array and readout hybrid prior to thinning process. After hybridization step, the pixels of 2-D arrays are thinned to about 5μm in thickness. This can be made, e.g. by removing the substrate using a $SF_6:SiCl_4$ backside dry etch through to the bottom AlGaAs etch stop layer. The thinning traps diffract-

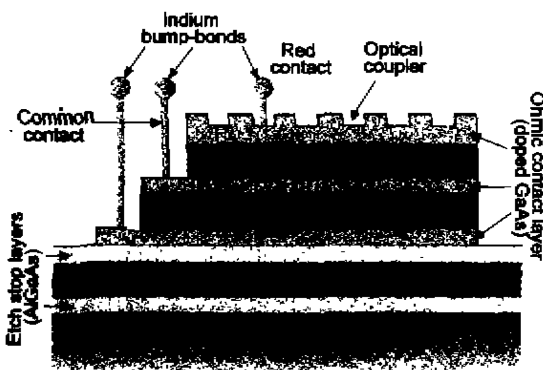

Fig. 15 Structure of two-color stacked QWIP (after Ref. 14)

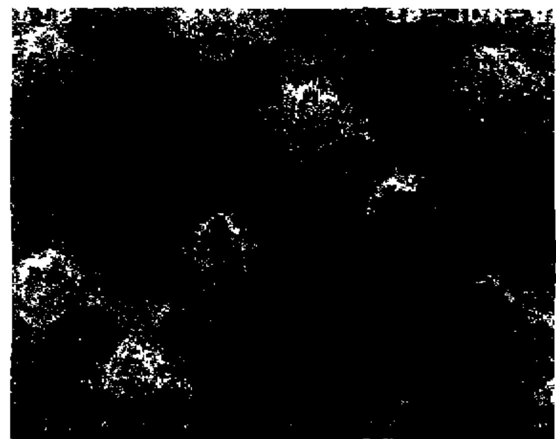

Fig. 16 Section of a two-color QWIP FPA after indium bump deposition (after Ref. 14)

ed light inside the illuminated pixels, increasing responsivity and eliminating crosstalk. The thinning also allows the detector array to stretch and accommodate the thermal expansion mismatch with the Si readout integrated circuit.

Typical operating temperature for QWIP detectors is in the region of 40~100K. Figure 17 shows the responsivity of both QWIPs at a temperature 40K and at an operating bias of 1.5V applied to common contact. The bias across each QWIP can be adjusted separately, although it is desirable to apply the same bias to both colors. As shown in Fig. 17, the responsivity of both QWIPs is around 300~350mA/W.

It appears that the complex two-color processing has not compromised the electrical and optical quality of either color in the two-color device since the peak quantum efficiency for each of the 20-period QWIPs was estimated to be ≈10% in comparison with a normal single-color QWIP with twice the number of periods which has a quantum efficiency of around 20%. A pixel operability for each color is >97% in comparison to the value of >99.5% routinely achieved for single-color QWIPs. The NEDT value was 24mK for the blue QWIP and 35mK for the red QWIP. The difference was assigned to the poor transmission properties of the optics in the 11.2μm band.

Two-color detectors that cover both MWIR and LWIR atmospheric windows are especially important in many applications. To cover MWIR range a strained layer InGaAs/AlGaAs material system is used. InGaAs in MWIR stack produces high in-plane compressive strain, which enhances the responsivity[24,25]. The MWIR/LWIR FPAs fabricated by

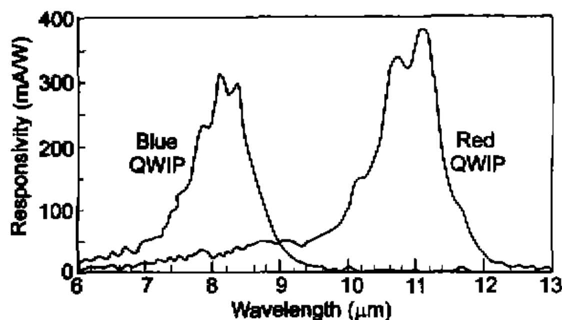

Fig. 17 Typical responsivity spectra at 40K and a common bias of 1.5V, recorded simultaneously for two QWIPs in the same pixel (after Ref. 14)

Fig. 18 Simultaneous images from 256×256 MWIR/LWIR QWIP FPAs. Note appearance of the filter and the soldering iron in the two bands (after Ref. 14)

Sanders consist of an 8.6μm GaAs/AlGaAs QWIP on top of 4.7μm strained InGaAs/GaAs/AlGaAs heterostructure. The fabrication process allowed fill factors of 85% and 80% for the MW and LW detectors. The first FPAs with this configuration had an operability in excess of 97%, and NETD value better than 35mK. The excellent imagery in each color is shown in Fig. 18. Note the appearance of the filter and the soldering iron in the two bands.

Recently, Gunapala *et al*[15,26]. have demonstrated the first 8~9 and 14~15μm two-color imaging camera based on a 640×486 dual-band QWIP FPA, which can be processed with dual or triple contacts to access the CMOS readout multiplexer. Single indium bump per pixel is usable only in the case of interlace readout scheme (i.e., odd rows for one color and the even rows for the other color) which uses an existing single color CMOS readout multiplexer. However, the disadvantage is that it does not provide a full fill factor for both wavelength bands.

The device structure, shown in Fig. 19, consists of a 30-period stack (500Å AlGaAs barrier and a 60

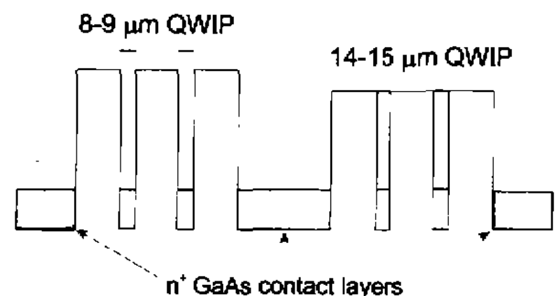

Fig. 19 Conduction band diagram of the LWIR and VLWIR two-color detector (after Ref. 15)

Å GaAs well) of very long wavelength IR (VLWIR) structure and a second 18-period stack (500 Å AlGaAs barrier and a 40 Å GaAs well) of LWIR structure separated by a heavily doped 0.5μm thick intermediate GaAs contact layer. The VLWIR QWIP structure has been designed to have a bound-to-quasibound intersubband absorption peak at 14.5μm, whereas the LWIR QWIP structure has been designed to have a bound-to-continuum intersubband absorption peak at 8.5μm, since phtocurrent and dark current of the LWIR device structure are relatively small compared to the VLWIR portion of the device structure. The GaAs well doping density of the LWIR stack was intentionally increased by a factor of two to compensate for the reduced number of quantum wells in the LWIR stack. The total current (dark current plus photocureent) of each stack was independently controlled (by position of the upper state, doping densities, number of periods) to obtain approximately equal total current from each MQW stack.

The peak responsivity of the LWIR detectors is 509mA/W at 8.4μm and bias $V_B=-2$V. The spectral width and the cutoff wavelength of the LWIR detectors are $\Delta\lambda/\lambda=16\%$ and $\lambda_c=9.1$μm, respectively. The responsivity of the VLWIR detectors peaks at 14.4μm and the peak responsivity of the detector is 382mA/W at $V_B=-2$V. The spectral width and the cutoff wavelength of the VLWIR detectors are $\Delta\lambda/\lambda=10\%$ and $\lambda_c=15$μm, respectively. The peak quantum efficiencies of LWIR and VLWIR detectors were 5.4% and 13.2%, respectively at operating bias of $V_B=-2$V. The peak detectivities of both detectors are shown in Fig. 20. The 8～9μm detectors have shown background limited performance (BLIP) at 70K operating temperature, at 300K background with $f/2$ cold stop. The 14～15μm detectors show BLIP with the same operating conditions at 45K.

Figure 21 shows schematic side view of the interlace dual-band GaAs/AlGaAs FPA. Two different 2-D periodic grating structures were designed to independently couple the 8～9μm and 14～15μm radiation into detector pixels in even and odd rows of the FPAs. The top 0.7μm thick GaAs cap layer was used to fabricate the light coupling 2-D periodic gratings for 8～9μm detector pixels, whereas the light coupling 2-D periodic gratings of the 14～15μm detector pixels were fabricated through LWIR MQW layers. In such a way, this grating scheme short circuited all 8－9μm sensitive detectors in all odd rows of the FPAs. The grating structure is fabricated by using standard photolithography and SF_6:BCl_3 selective dry etching. Next the LWIR detector pixels were fabricated by dry etching through the photosensitive GaAs/AlGaAs MQW layers into the 0.5μm thick doped GaAs intermediate contact layer. All VLWIR pixels in the even rows of FPAs were short circuited. All VLWIR deector pixels were fabricated by dry etching both MQW stacks into the 0.5μm thick heavily doped GaAs bottom contact layer. The 2-D grating reflectors on top of the detectors were then covered with Au/Ge and Au for ohmic contact and re-

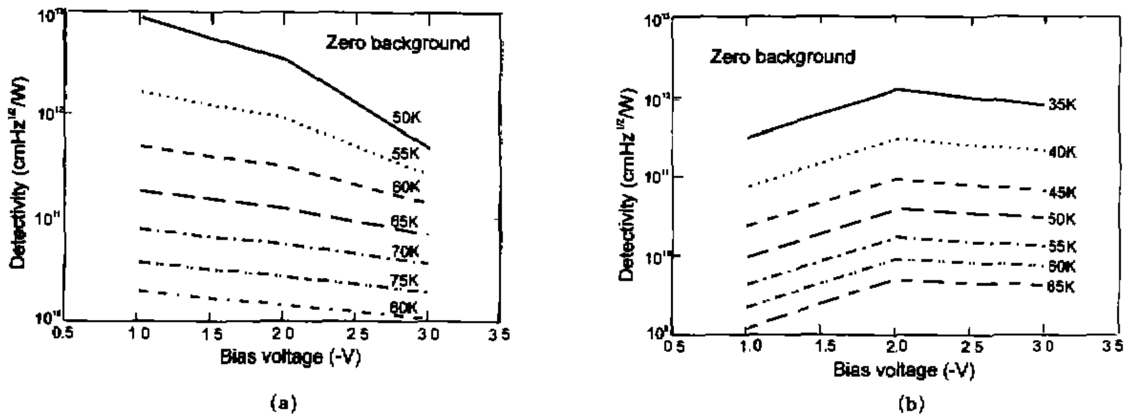

Fig. 20 Experimentally measured detectivities of LWIR (a) and VLWIR (b) detectors as a function of bias voltage at different operating temperatures (after Ref. 15)

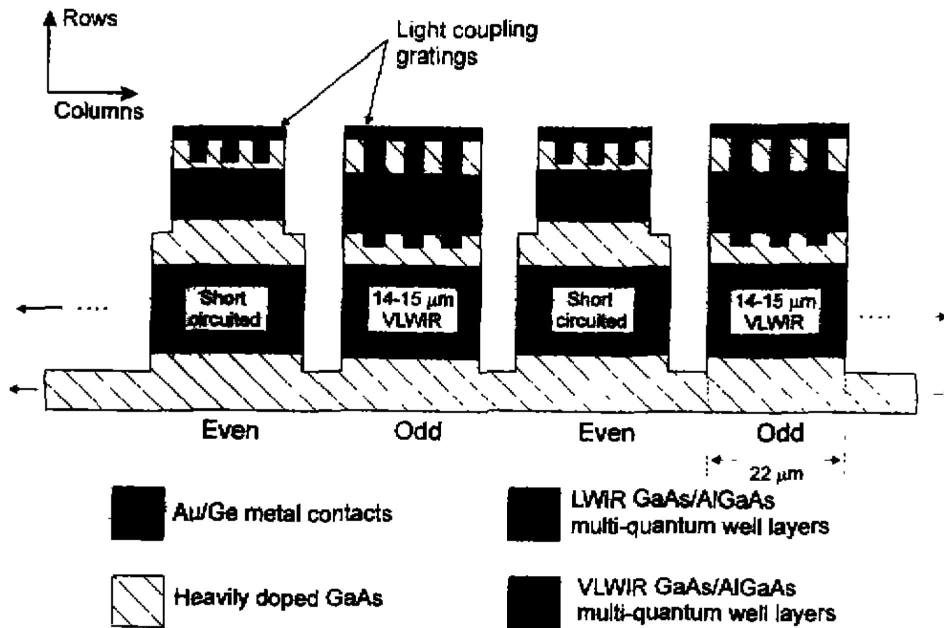

Fig. 21 Sttucture cross section of the interlace dual-band FPA (after Ref. 15)

flection. Indium bumps were then evaporated on top of the detectors for silicon readout circuit hybridization. After epoxy backfilling of the gaps between FPA detectors and the readout multiplexer, the substrate was thinned. In the first step of the thinning process an approximately 500μm thick GaAs was removed using abrasive polishing or diamond turning. Then bromine-methanol chemical polishing was used to remove approximately 100μm. Next wet chemical etchant was used to reduce the substrate to several micrometers and $SF_6:BCl_3$ selective dry etchant was used as the final etch. As a result, the remaining GaAs/AlGaAs material contains only the QWIP pixels and a very thin membrane (≈1000Å). This allows to adapt to the thermal expansion and contraction coefficient of the silicon readout multiplexer, completely eliminates the thermal mismatch problem between the silicon readout and the GaAs based detector array, completely eliminates pixel-to-pixel crosstalk, and finally, a significant enhancement in optical coupling of IR radiation into QWIP pixels[27]. The FPA was backilluminated through the flat thinned substrate membrane.

The 640×486 GaAs/AlGaAs gave excellent images with 99.7% of the LWIR pixels and 98% of VLWIR pixels working, demonstrating the high yield of GaAs technology (the operability is defined as the percentage of pixels having noise equivalent differential temperature less than 100mK at a 300K blackbody). At temperatures below 70K, the signal-to-noise ratio of the LWIR detector pixels is limited by array non-uniformity, multiplexer readout noise, and photocurrent noise (for $f/2$ cold stop). At temperatures above 70K, temporal noise due to the QWIP's higher dark current (thermionic emission) becomes the limitation. At temperatures below 40K, the signal-to-noise ratio of the VLWIR detector pixels is limited by array non-uniformity, multiplexer readout noise, and photocurrent noise. The QWIPS detectors are high impedance devices. The differential resistance of both LWIR and VLWIR pixels at −2V bias is greater than $7\times10^{11}\Omega$ at 40K and detector capacitance is 3×10^{-14}F. The detector currents of LWIR and VLWIR detectors are 2.6×10^{-15} and 2.5×10^{-12}A, respectively at 40K. Charge injection efficiency into the CMOS readout multiplexer exceeds 90% at a 30Hz frame rate.

The performances of dual-band FPAs were tested at a background temperature of 300K, with $f/2$ cold stop, and at 30Hz frame rate. The mean value of

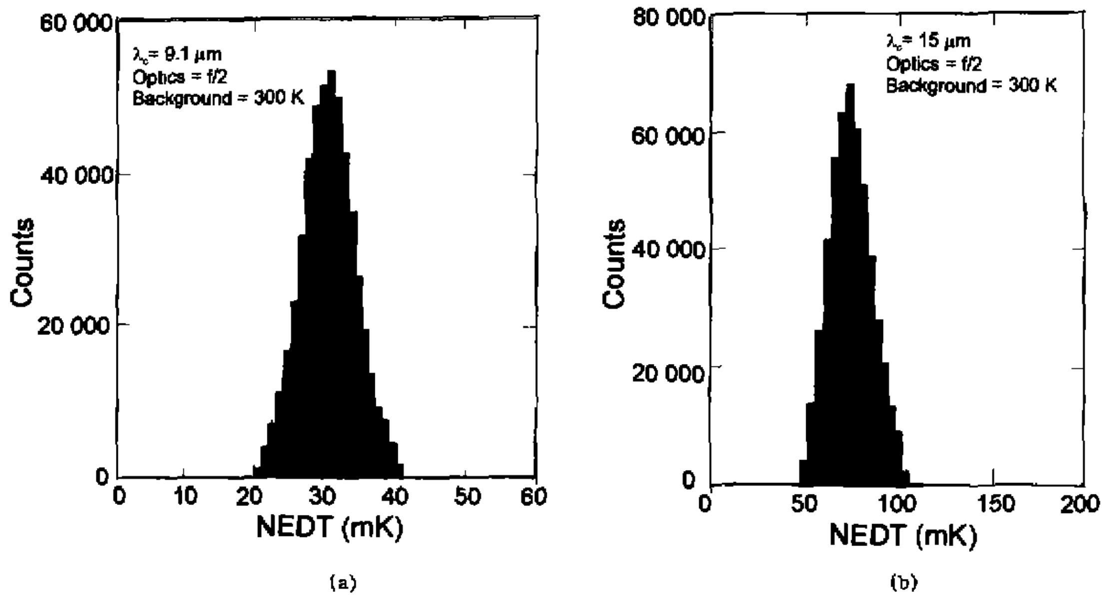

Fig. 22 The uncorrected NEDT histograms of 8~9μm detector pixels (a) and 14~15μm detector pixels (b) of the 640×486 dual-band FPA. The mean *NEDT* are: 29mK for LWIR FPA and 74mK for VLWIR FPA (after Ref. 15)

the LWIR FPA quantum efficiency is 12.9% at operating temperature of T=40K, bias V_B=−2V. This integrated quantum efficiency includes 30% substrate reflection and 85% FPA fill factor. The uncorrected non-uniformity (i.e., sigma/mean) of the quantum efficiency histogram is 2%. The mean quantum efficiency of 14~15μm detector pixels in the FPA is 8.9%, and the uncorrected quantum efficiency non-uniformity is about 1%.

The estimated NEDT of LWIR and VLWIR detectors at 40K are 36 and 44mK, respectively. Due to BLIP, the estimated and experimentally obtained NEDT values of the LWIR detectors do not change significantly at temperatures below 65K. The experimentally measured values of LWIR NEDT equal to 29mK are lower than the estimated ones [see Fig. 22 (a)]. This improvement is attributed to the 2-D periodic grating light coupling efficiency. However, the experimental VLWIR NEDT value [see Fig. 22(b)] is higher than the estimated value. It is probably a result of the inefficient light coupling at 14~15μm region, readout multiplexer noise, and noise of the proximity electronics. At 40K the performances of both bands detector pixels are limited by photocurrent noise and readout noise.

3 Conclusions

QWIP cannot compete with HgCdTe photodiode as the single device especially at higher temperature operation(>70K) due to fundamental limitations associated with intersubband transitions. However, the advantage of HgCdTe is less distinct in temperature range below 50K due to problems involved in HgCdTe material (p-type doping, Shockley-Read-recombination, trap-assisted tunnelling, surface and interface instabilities). Even though QWIP is a photoconductor, several of its properties such as high impedance, fast response time, long integration time, and low power consumption, well comply with the requirements of fabrication of large FPAs. Due to the high material quality at low temperature, QWIP has potential advantages over HgCdTe for VLWIR FPA applications in terms of the array size, uniformity, yield and cost of the systems.

Both HgCdTe detectors and quantum well GaAs/AlGaAs photodetectors offer wavelength flexibility from MWIR to VLWIR and multicolor capability in these regions. We have reviewed performance

data for dual band HgCdTe and QWIP hybrid FPAs. The performance data confirm that all the key features of both types of detectors function as expected and designed. The main challenges facing both dual-band devices are more complicated device structures, thicker and multilayer material growth, and more difficult fabrication, especially when the array size gets larger and pixel size gets smaller. In the case of HgCdTe devices, the multiple p-n junctions are required more difficult in material growth, device fabrication and passivation. The major challenge for QWIP is developing broadband or multicolor optimal coupling structures that permit efficient absorption of all required spectral bands. The second issue that impedes the QWIP's performance at higher temperature is large dark current.

Several companies plan to advance simultaneous dual-band FPA technology to larger array sizes, smaller pixels cells, and higher performance, especially that required for low background applications. For strategic applications, special variants of dual-band input circuits are designed for improved performance at lower background photon fluxes.

Most commercial market probably will be dominated by uncooled IR FPAs, except for medical applications where high resolution and accuracy are needed. However, uncooled detectors developed so far are less sensitive than the cooled detectors. It also has no intrinsic multicolor capability.

Acknowledgements

This work was partially supported by the Polish State Committee for Scientific Research under grant number PBZ 28.11/P6.

REFERENCES

[1]Norton P R. Status of infrared detectors, *Proc. SPIE*, 1998,**3379**: 102—114

[2]Norton P R. Infrared detectors in the next millennium, *Proc. SPIE*,1999,**3698**: 652—665

[3]Tidrow M Z, Beck W A, Clark W W, *et al.* Device physics and focal plane array applications of QWIP and MCT, *Opto-Electr. Rev.* ,1999,**7**:283—296

[4]Rogalski A. Assessment of HgCdTe photodiodes and quantum well infrared photoconductors for long wavelength focal plane arrays,*Infrared Phys. Technol.* ,1999,**40**: 279—294

[5]Rajavel R D, Jamba D M, Wu O K, *et al.* High performance HgCdTe two-color infrared detectors grown by molecular beam epitaxy, *J. Crystal Growth*, 1997, **175**: 653—658

[6]Rajavel R D, Jamba D M, Jensen J E, *et al.* Molecular beam epitaxial growth and performance of integrated multispectral HgCdTe photodiodes for the detection of mid-wave infrared radiation, *J. Crystal Growth*, 1998,**184** : 1272—1278

[7]Rajavel R D, Jamba D M, Jensen J E, *et al.* Molecular beam epitaxial growth and performance of HgCdTe-based simultaneous-mode two-color detectors, *J. Electron. Mater*, 1998,**27**: 747—751

[8]Johnson J L. Two-color HgCdTe devices for multispectral applications, *Extended Abstracts of the* 1999 *U. S. Workshop on the Physics and Chemistry of* **I**-Ⅵ *Materials*, September 22—24,1999, Las Vegas, pp. 101—104(1999)

[9]Reine M B, Norton P W, Starr R, *et al.* Independently-accessed back-to-back HgCdTe photodiodes: a new dual-band infrared detector, *J. Electron. Mater.* ,1995,**24**: 669—679

[10]Mitra P, Barnes S L, Case F C, *et al.* MOCVD of bandgap-engineered HgCdTe p-n-N-P dual-band infrared detector arrays, *J. Electron. Mater*, 1997,**26**: 482—487

[11]Reine M B, Hairston A, O'Dette P, *et al.* Simultaneous MW/LW dual-band MOCVD HgCdTe 64 × 64 FPAs, *Proc. SPIE*, 1998,**3379**: 200—212

[12]Pollehn H K, Ahearn J. Multi-domain smart sensors, *Proc. SPIE*,1999,**3698**: 420—426

[13]Beck W A, Faska T S. Current status of quantum well focal plane arrays,*Proc. SPIE*,1996,**2744**: 193—206

[14]Whitaker T. Sanders' QWIPs detect two color at once, *Compound Semiconductors*,1999,**5**(7): 48—51

[15]Gunapala S D, Bandara S V, Sigh A, *et al.* 8~9 and 14~15μm two-color 640×486 quantum well infrared photodetector (QWIP) focal plane array camera,*Proc. SPIE*, 1999,**3698**: 687—697

[16]Campbell J C, Dentai A G, Lee T P, *et al.* Improved two-wavelength demultiplexing InGaAsP photodetector, *IEEE J. Quantum Electron*,1980,**QE-16**: 601

[17]Wilson J A, Patten E A, Chapman G R, *et al.* Integrated two-color detection for advanced FPA applications,*Proc. SPIE*,1994,**2274**: 117—125

[18]Johnson S M, Rhiger D R, Rosbeck J P, *et al.* Effect of dislocations on the electrical and optical properties of long-wavelength infrared HgCdTe photovoltaic detectors, *J. Vac. Sci. Technol.* ,1992,**B10**: 1499—1506

[19]Jozwikowski K, Rogalski A. Effect of dislocations on performance of LWIR HgCdTe photodiodes, *Extended Abstracts of the* 1999 *U. S. Workshop on the Physics and Chemistry of* Ⅱ-Ⅵ *Materials*, September 22—24, 1999, Las Vegas,pp. 95—98

[20]Andersson J Y, Lundqvist L, Paska Z F. Quantum efficiency enhancement of AlGaAs/GaAs quantum well infrared detectors using a waveguide with a grating coupler, *Appl. Phys. Lett.* ,1991,**58**: 2264—2266

[21]Sarusi G, Levine B F, Pearton S J, *et al.* Improved performance of quantum well infrared photodetectors using

random scattering optical coupling, *Appl. Phys. Lett.*, 1994, **64**: 960—962

[22]Chen C J, Choi K K, Tidrow M Z, *et al.* Corrugated quantum well infrared photodetectors for normal incident light coupling, *Appl. Phys. Lett.*, 1997, **68**: 1446—1448

[23]Li S S, Wang Y H. Novel grating coupled and normal incidence Ⅲ-V quantum well infrared photodetectors with background limited performance, in *Quantum Well Intersubband Transition Physics and Devices*, edited by H. C. Liu, B. F. Levine, and J. Y. Anderson, Dordrecht; Kluwer Academic Publishers, 1994, 29—42

[24]Tidrow M Z, Chiang J C, Li S S, *et al.* A high strain two-stack two-color quantum well infrared photodetector, *Appl. Phys. Lett.*, 1997, **70**: 859—861

[25]Bois Ph, Costard E, Duboz J Y, *et al.* Technology of multiquantum well infrared detectors, *Proc. SPIE*, 1997, **3061**: 764—771

[26]Gunapala S D, Bandara S V, Liu J K, *et al.* Quantum well infrared photodetector research development at Jet Propulsion Laboratory, *Proc. SPIE*, 1998, **3379**: 382—395

[27]Gunapala S D, Bandara K M S V. Recent development in quantum-well infrared photodetectors, *Thin Films*, New York; Academic Press, 1995, Vol. 21 pp. 113—237